Histol Histopathol (2021) 36: 753-764

http://www.hh.um.es

Histology and Histopathology
From Cell Biology to Tissue Engineering

ORIGINAL ARTICLE **Open Access**

Sequential osseointegration from osseohealing to osseoremodeling - Histomorphological comparison of novel 3D porous and solid Ti-6Al-4V titanium implants

Alice Frosch[1], Sebastian Krohn[2], Gottfried Buchhorn[1], Wolfgang Lehmann[1], Karl-Heinz Frosch[3], László Füzesi[4] and Stephan Frosch[1]

[1]Department of Trauma Surgery, Orthopedics and Plastic Surgery, University Medical Center Göttingen, [2]Department of Prosthodontics, University Medical Center Göttingen, Göttingen, [3]Department of Trauma and Orthopedic Surgery, University Medical Center Hamburg - Eppendorf, Hamburg and [4]Department of Pathology, University Medical Center Göttingen, Göttingen, Germany

Summary. In the present study, we analyzed the histological characteristics of osseointegration of an open-porous Ti-6Al-4V material that was produced in a space holder method creating a 3-D through-pores trabecular design that mimics the inhomogeneity and size relationships of trabecular bone in macro- as well as microstructure. Pairs of cylindrical implants with a porosity of 49% and an average pore diameter of 400 μm (PI) or equal sized solid, corundum blasted devices (SI) as reference were bilaterally implanted press fit in the lateral condyles of 16 rabbits. Histological examination was performed after 4 weeks of short-term osseohealing and 12 weeks of mid-term osseo-remodeling and we summarized the criteria for sequential osseointegration. After 4 weeks, osteoid had already been largely replaced by mineralized woven bone in both types of implants but was only represented to a greater extent in the deeper pores of PI. The cortical as well as trabecular region showed regular osseohealing with excessive and spatially undirected formation of immature woven bone. A dense bone mass was found in the cortical area, while in the trabecular region the bone mass was reduced distinctly, presenting large lacuna-like recesses and a demarcating trabecular structure. The pores near the implant surface contained more mineralized woven bone than the deeper pores. After 12 weeks, the osseoremodeling was largely completed with a physiological maturation to lamellar bone. The newly formed bone mass increased for PI and SI compared to the 4-week group and osteoid was only detectable in the deeper pores. The inhomogeneous trabecular design of the pores enables an excellent ingrowth of mineralized lamellar bone after remodeling to a pore depth of 1800 μm, which proves a functional load transfer from the surrounding bone into the implant. According to the concept of osseointegration by Branemark and Albrektsson, the histological evaluation confirms a successful, superior osseointegration of the presented porous properties improving long-term implant stability. The presented study protocol allows an excellent evaluation and comparison of the sequential osseointegration from short-term osseohealing to mid-term osseoremodeling.

Key words: Histology, Porous Titanium Implants, Osseointegration, Osseohealing, Osseoremodeling, Woven Bone, Lamellar Bone, Osteoid

Introduction

Osseointegration as a biological concept describes the incorporation, fixation and stability of a foreign body in vital bone during functional stress (Branemark et al., 1977; Boyan et al., 1996). A number of factors are decisive for successful long-term results, such as the selection of the material for the bone replacement, the design and the surface quality of the implant, the anatomical location of the implantation site, the vitality of the bone, surgical techniques, but also the patient's compliance (Albrektsson and Zarb, 1993; Albrektsson and Wennerberg, 2019). The excellent properties of titanium and its alloys, with a high strength-to-weight ratio, high corrosion resistance, low allergenicity and the ability to osseointegrate are well-known and make titanium the most commonly used material for

Corresponding Author: Dr. Stephan Frosch, Department of Trauma Surgery, Orthopedics and Plastic Surgery, University Medical Center Göttingen, Robert-Koch-Straße 40, 37075 Göttingen, Germany. e-mail: Stephan.Frosch@med.uni-goettingen.de

DOI: 10.14670/HH-18-333

Abbreviations. PI, porous implant; SI, solid implant.

orthopedic and dental implants (Long and Rack, 1998; Simsek and Ozyurek, 2019). Porous titanium implants have the advantage of a lower modulus of elasticity, which is closer to that of the bone, and an associated lower risk of developing stress shielding than implants made of solid titanium (Wolff, 1892; Sumner et al., 1998). Furthermore, porosity enhances the osteoconductive and osteoinductive abilities of the implant, supports biological anchorage and facilitates a higher bone-implant contact (BIC) at the surface (Rosa et al., 2009; Kim et al., 2013; Bencharit et al., 2014). However, there is no agreement on which structural properties such as porosity and size of the pores would best promote osseointegration. In the present study, we evaluate the short-term and mid-term osseointegration of a 3-D through-pores Ti-6Al-4V material with an average pore diameter of 400 μm and a porosity of 49% that mimics the inhomogeneity and size relationship of trabecular bone in macro- and microstructure (Hartmann, 2012; Cheng et al., 2017). Both types of implants were subjected to a previous comparative push-out study, which demonstrated a superior biomechanical osseous fixation of the porous implant compared to the solid control group (Frosch et al., 2020).

Biomechanical push-out and pull-out test are frequently used methods for characterizing contact phenomena as an indication of the degree of osseointegration. However, they cover only the mechanical aspect of osseous integration and the individual parameters and test arrangements vary widely, which can impair the results and make comparison with other studies more difficult (Berzins and Sumner, 2000). For example, a slight tilt of samples relative to the axis of symmetry of the driving push-out tool will conduct heterogeneous separation of bone tissue from implant surfaces and lead to erroneously higher data ("catching effect") (Frosch et al., 2020). A thorough histological examination is rare in the literature, but facilitates a genuine and detailed assessment of osseointegration. Only regular, physiological osteogenesis from initial osseohealing to later osseoremodeling facilitates long-term implant stability. Furthermore, a reliable comparability with other studies is possible regardless of the material composition, shape and size of the implants, biomechanical test arrangements and other individual parameters.

The aim of the present study was to analyze the sequential osseointegration of the presented Ti-6Al-4V porous implant (PI) by histomorphological characterization of short-term osseohealing and mid-term osseoremodeling in an *in vivo* animal experiment and compare the results to a solid Ti-6Al-4V titanium implant (SI). Particular attention was paid to demonstrate a regular osteogenesis in the cortical and trabecular region as well as intraporous.

Materials and methods

Implant materials

We used two titanium implants with different surface and structure characteristics, PI as well as SI, respectively. Cylinders with a central boring of both implant types were made from Ti-6Al-4V (ISO 5832-3 and ASTM F136) and match in geometry in order to enable comparison and to allow a uniform implantation process (Fig. 1). Each implant had a height of 7.0 mm and a diameter of 5.6 mm with a central 2.0 mm boring. The surface of the SI was grit blasted in a standard procedure using a corundum with a grain size of 1000 μm to produce a rough surface. The PI were manufactured in a basic space-holder process (Fraunhofer Institute for Manufacturing Technology and Advanced Materials [IFAM], Bremen, Germany) and based on the work of Bram, Bobyn and Rausch (Bobyn et al., 1980; Rausch et al., 2000; Bram et al., 2004, 2013; Hartmann, 2012). The average pore size of 400 μm was established by sieving paraformaldehyde spheres using an analytic sieve shaker (AS 200 control g, ISO 9001, Retsch Company, Haan, Germany). The mixing ratio of

Fig. 1. Porous (left) and solid, blasted (right) Ti-6Al-4V implants.

the titanium granules (powder fraction of 22 to 45 μm) to the quantity of spacer beads and to a wax binder was established to 20:8:1 in order to achieve a porosity of 49%. Samples of the desired shape were produced in a hydraulic press and sintered. After turning in a lathe to final dimensions and central boring, SI were grit blasted with 1000 μm corundum and PI were blasted with nitrogen ice granules to remove particles, impurities, and to free blocked pores.

Animals

Animal experiments and all aspects related to the care and treatment of the animals were approved by local and federal authorities (LAVES, 28. 04. 2010, AZ 33.14-42502-04-10/0059). 16 female rabbits (Chinchilla-Bastard, Charles River GmbH, Sulzfeld, Germany) with an age of 12 to 14 weeks and a body weight not under 3 kg were included in the study. The staff and the veterinarian regularly observed the animals for species-appropriate, pain free behavior. Two animals were excluded, one from evaluation due to lack of press-fit (instrumentation problem), one due to deep infection after bite wound.

Implantations

Both implant types were randomly distributed bilaterally to the lateral femoral condyles of the animal. Animals received preliminary i. m. anesthesia 0.3 ml (10 mg) Xylazin and 0.5 ml/kg (50 mg) Ketanest. The lateral knees were clean shaven, the skin was disinfected and covered sterile. Attention was paid to work sterile during operation. Continuous infusion of general anesthesia (5 ml Xylazin + 5 ml Ketanest + 40 ml NaCl at 1.7 ml/kg/h) was established using an ear vein. Skin incision over the lateral femoral condyle and exposure of bone proximally of the growth plate allowed preparation of a cylindrical bore. A bediamonded hollow grinder (Fa. Articomed, Schlüchtern, Germany) with an outer diameter of 5.4 mm was used to reach a depth of 7.0 mm. Permanent cooling with physiologic saline was applied. The central bone block was extracted and the bottom of the bore was leveled. The implant was carefully centered and press-fit impacted until the lateral implant side was at best possible plane with the cortical bone (Fig. 2). Wound closure in layers was followed by an intracutaneous seam and skin surface disinfection. An antibiotic (0.5 ml Penstrep) was given perioperatively once and analgesic (Rimadyl 0.1 ml/kg) for the following 3 days.

Sampling and Thin-ground Process

The animals were randomized into two groups. Eight animals each were sacrificed after 4 and 12 weeks with injection of Embutramid (0.3 ml/kg, Intervet, Köln, Germany). The femora were harvested and dissected from the soft tissues with special care not to impair the bone surfaces. All specimens were shock-frozen by immersion in dry ice cooled iso-pentane and stored at -20°C (Diefenbeck et al., 2011). For further processing, the specimens were thawed at room temperature overnight and stored in a buffered 4% formalin solution. The fixed specimens were trimmed, washed in 0.1 M phosphate buffer solution and dehydrated in ascending alcohol series. To ensure an accurate evaluation as part of the thin-ground process, it was important to achieve a cut exactly perpendicular to the axis of symmetry of the implant without any angular deviation. Therefore, the implant had been provided with a central boring with a diameter of 2 mm that strictly followed the longitudinal axis of the implant. A close-fitting spike wire was introduced into the central boring along the longitudinal axis of the implant. The wire was predefined connected to a jig of the cutting machine (Exact Sectioning System, Messner, Oststeinbek, Germany) ensuring precise saw cuts perpendicular to the axis of the implants without any angular deviation after removal of the wire. For histomorphology, tissue thin cut slices should reproducibly show a circular projection of the implant cross section. A cold-curing polymethyl methacrylate embedding medium "Technovit® 9100" (Heraeus Kulzer, Wehrheim, Germany) was used. The saw microtome SP1600 (Leica Mikrosysteme Vertriebs GmbH, Bensheim, Germany) was used to cut the specimens, followed by grinding the specimens down to a thickness of 25 μm.

Histological analysis

The histological evaluation of the peri-implant and intraporous region was carried out along the longitudinal axis of the implants. In order to perform a separate evaluation according to the anatomical position of the implant, four sectional planes were placed along the longitudinal axis of the implant. Sections 1 and 2 were placed in the cortical area and sections 3 and 4 in the trabecular area of the implant in the distal femur (Fig. 3).

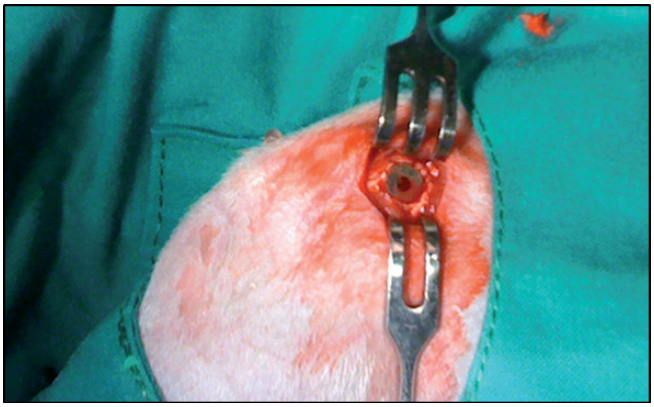

Fig. 2. Intracondylar position of a titan cylinder, flush with the outer lateral cortical layer.

Histological staining was carried out according to Smith and Karadgianes (Smith and Karagianes, 1974). The polished specimens were pretreated with methylene blue and then stained with alizarin red (Dahl, 1952). For the staining process, the cut preparations were immersed in the methylene blue solution, which had been heated to 80°C for 30 seconds, and then rinsed thoroughly with distilled water. Drying was carried out at room temperature for three to four hours. Afterwards, the pretreated preparations were placed in alizarin red solution for 40 seconds and then again washed thoroughly with Aqua dest. The preparations were dried at room temperature for 24 hours. The digitization of the sections was carried out by a fully automated microscope (Axiovert 200M, Carl Zeiss, Oberkochen, Germany) connected to a digital camera (Axiocam, Carl Zeiss, Oberkochen, Germany). The histological evaluation was performed using an image editing program (Adobe Photoshop® Elements 7). With the help of the program, a concentric circle around the transverse axis of the implants with a radial distance from the implant surface of +1000 μm (diameter of 7.6 mm) was projected into the digitized histological sections. The circular area formed the area of interest in which the examinations were carried out. The histological staining allowed discrimination between mineralized (brown) and non-mineralized (blue) bone. The histomorphological criteria of different maturation states of bone as osteoid, woven and lamellar bone have been reviewed according to the literature (Fig. 4) (Marotti et al., 1979; Eriksen et al., 1984; Andrew and Rosenberg, 2004; Shapiro, 2008; Vigorita, 2015; Shapiro and Wu, 2019).

Statistics

The distribution of the parameters bone area and BIC was described by its mean and standard deviation separately for implant (SI vs. PI), weeks (4 vs. 12) and sections (cortical vs. trabecular). The effect of implant

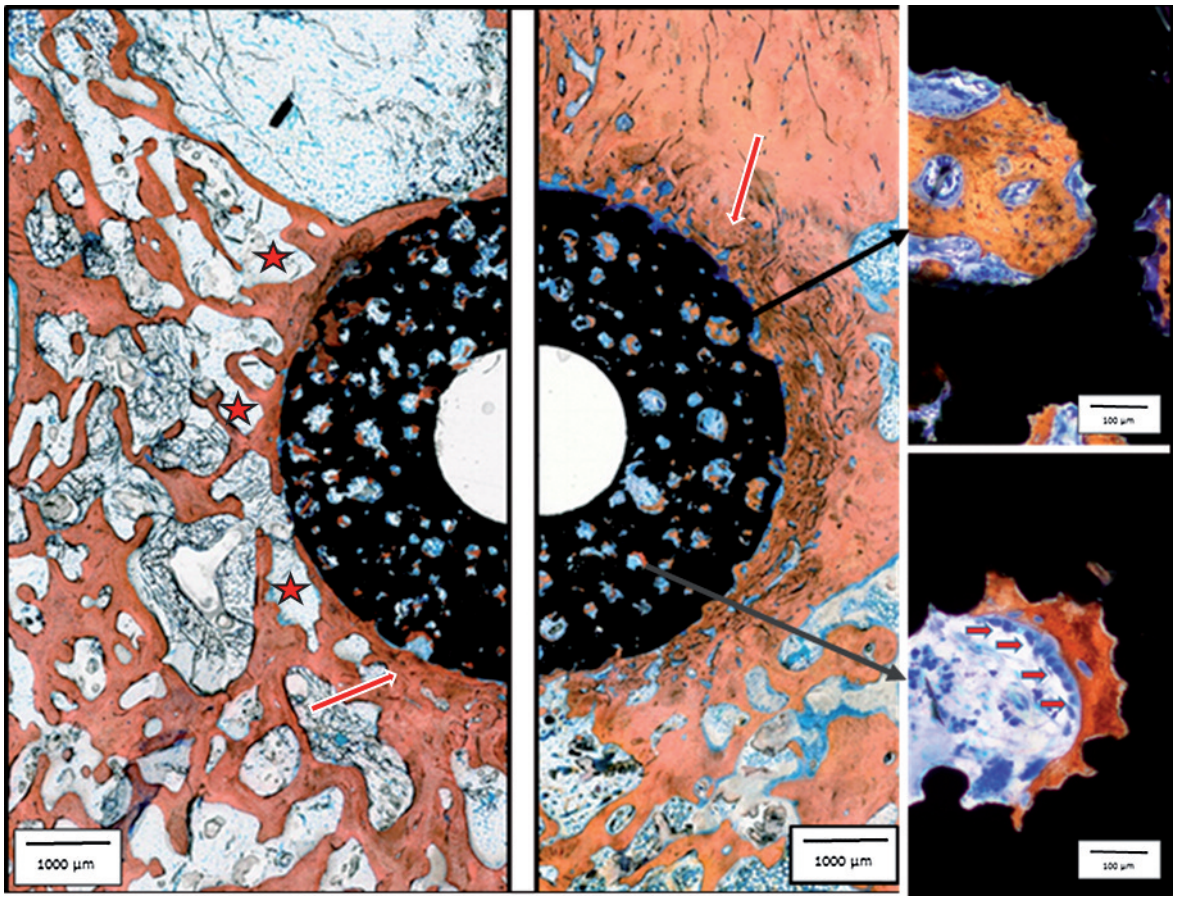

Fig. 3. Porous implant according to the anatomical position 4 weeks after implantation: cortical section (middle) and trabecular section (left). Cell-rich newly formed woven bone (dark brown, red arrows) vs. genuine lamellar bone (light brown). More mineralized woven bone and less osteoid in the superficial pores (right, top) and vice versa in the deeper pores. Surface osteoblasts forming bone matrix (right top and bottom, red small arrows). Reduced amount of trabecular bone area compared to the cortical region (left, middle). Large lacuna-like recesses in the trabecular region, peri-implant (red stars). Stained with methylene blue - alizarin red. x 20 (left, middle); x 40 (right bottom, top).

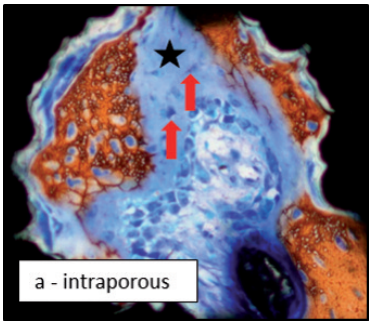

Osteoid (**a**, black star)
- collagen type I, extracellular bone matrix, noncollagenous proteins (Vigorita, 2015)
- unmineralized portion of the bone synthesized and deposited by osteoblasts
- osteoid begins to calcify about ten days after deposition (Vigorita, 2015)
- linear rate of osteoid apposition of 0,4-1,8 *μ*m/day (Marotti et al., 1979)

Osteoblasts can be morphologically divided into mesenchymal and surface osteoblasts according to their function and position (Shapiro, 2008, Andrew and Rosenberg, 2004).

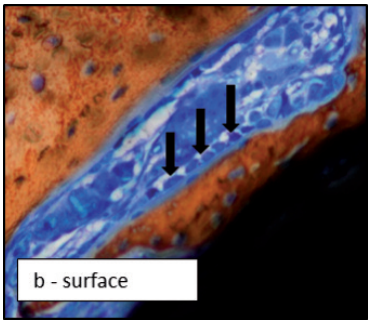

I *mesenchymal osteoblasts* (**a**, red arrows)

- undifferentiated mesenchymal cells differentiate to osteoblasts and secrete collagen fibrils in a 360 degree direction in random pericellular array (Shapiro, 2008)
- large cells with a round to oval shape, large cell nuclei and basophilic cytoplasm (Andrew and Rosenberg, 2004)
- first stages of bone formation
- no preexisting bone matrix

II *surface osteoblasts* (**b**, black arrows)

- array themselves only along the woven bone surface
- large epithelial cells with a flat appearance, large cell nuclei and narrow cytoplasm (Andrew and Rosenberg, 2004)
- secrete collagen fibrils only onto the pre-existing bone surface (Shapiro and Wu, 2019)
- secrete collagen parallel or lamellar orientation

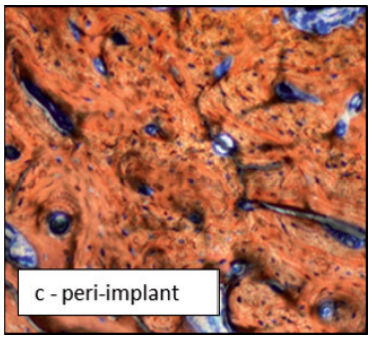

Woven bone represents an immature mineralized precursor of the mature lamellar bone **(c)**.
- mesenchymal and surface osteoblasts were present in larger numbers per unit area (than cells of lamellar bone) (Shapiro, 2008)
- surface osteoblasts array themselves only along the woven bone surface and secrete collagen fibrils onto the bone surface on the basal side of the osteoblasts (Shapiro and Wu, 2019)
- mesenchymal osteoblasts are surrounded by a randomly oriented, loosely packed in mineralized matrix and continue to synthesize matrix (image a, red arrows)
- when the osteoblast is surrounded by mineralized bone tissue and no more osteoid is produced (inactive), the transformation into an osteocyte is complete (Marotti et al., 1979)
- increased cellularity and irregular spatial distribution of the osteocytes in mineralized immature bone matrix **(c)**
- isolated evidence of osteoclasts (large multinucleated cell with abundant cytoplasm) (Eriksen et al., 1984)

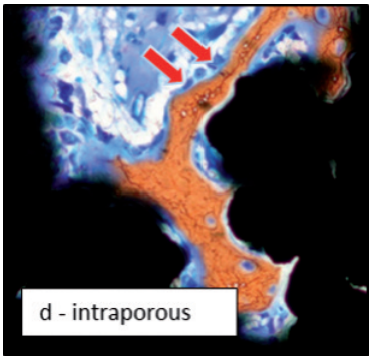

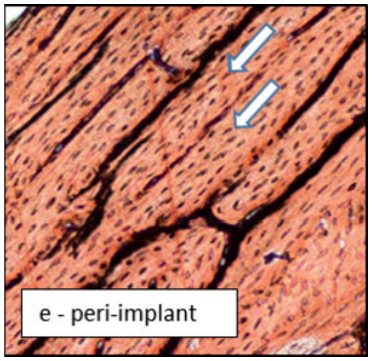

Lamellar bone presents a mature mineralized bone

- less cellular than woven bone (lower numbers per unit area) (Shapiro, 2008)
- collagen fibrils are closely packed and clustered in parallel arrays
- less active surface osteoblasts aligned in a linear array (often only one cell in depth) and deposit collagen in a unidirectional and in a parallel array (**d**, red arrows)
- lamellar bone osteocytes are elongated and elliptical in shape and have their long axes parallel to the lamellae (**e**, white arrows)
- osteons with central Haversian blood vessels, concentrically arranged with lamellae (Fig. 9)
- bone remodeling begins with osteoclasts that form resorption cavities (Howship's Lacuna) (Fig 5) (Eriksen et al., 1984)
- cement lines occur in the interface between completed and beginning new bone formations as part of remodeling (Fig. 6) (Vigorita, 2015)
- osteoclast cutting cones and resorb the dense cortical bone for vessel ingrowth (Fig. 6)

Fig. 4. Criteria of sequential osseointegration.

(SI vs. PI) in cortical and trabecular position and elapse time (4 vs. 12 weeks) were studied by analysis of variance (ANOVA). The significance level was set to α=5% for all statistical tests. All analyses of variance for repeated measures were performed with the statistic software R (version 3.0.2, www.r-project.org) using the R-package 'lme4' and 'lmerTest'.

Results

All histological slides showed a thin and uniform thickness sufficient for transmitted light microscopy and a coloration corresponding to the standard after pretreatment of the specimens with methylene blue and alizarin. In the microscopic evaluations, the bone was able to be distinguished from non-osseous tissue such as connective tissue or fatty tissue.

4-week group

In the cortical region, osteoid has already been largely replaced by mineralized woven bone in SI and PI, but the interstitial spaces were essentially filled with osteoid in the peri-implant region (Fig 3). There were osteoblasts walled-in in osteoid and active surface osteoblasts that were arrayed next to bone formations synthesizing osteoid (Fig. 4). Since the mineralized bony structure was already formed peri-implant, the predominant surface osteoblasts were arrayed along the woven bone surface (Fig. 5). Intraporous, the amount of osteoid increased with increasing pore depth and the ratio of osteoid to mineralized bone was reversed compared to the peri-implant region (Fig. 3). The osteogenesis appears less advanced than peri-implant and accordingly the mesenchymal walled-in osteoblasts predominate in contrast to the peri-implant region.

Newly formed woven bone surrounded both types of implants as a sign of primary osseohealing (Fig. 3). The woven bone showed an increased cellularity of immature osteocytes with oval and broad cytoplasm (Figs. 3, 4). The osteocytes were distributed irregularly and the collagen fibers of the bone matrix were arranged in coarse, undirected bundles in the bone matrix. Numerous capillaries were interposed. Sporadic osteoclasts could also be identified (Fig. 5). The presence of osteoblasts and osteoclasts confirms the simultaneous process of extension and degradation of bone formation as part of osseohealing and the beginning osseoremodeling (Fig. 5). The interface between the newly formed woven bone and the surrounding genuine bone was clearly visible (Fig. 3).

In the PI, the new bone formation continued from the implant surface into the pores. The degree of differentiation of bone tissue in the superficial pores corresponded to the peri-implant region (Fig. 3). However, a depth-dependent degree of differentiation of the newly formed bone from the superficial to the deeper pores was recognizable. The pores near the implant surface contained more mineralized woven bone than the deeper pores, where the proportion of non-mineralized osteoid was higher (Fig. 3).

In the trabecular region, the osteoid distribution is similar to that of the cortical region with no differences in size, shape or differentiation of the osteoblasts. The newly formed trabeculae already resembled mature trabecular structures to some extent and consisted mainly of undirected woven bone, which was less dense peri-implant than the the corresponding cortical structures (Fig 3). In contrast to the cortical sections, woven bone disclosed larger, bone-free recesses in the

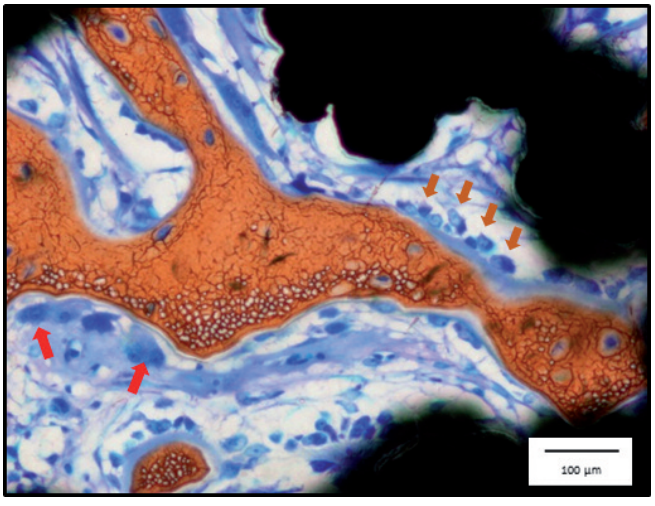

Fig. 5. Intraporous region in the trabecular section 4 weeks after implantation. Cell-rich woven bone (brown). Osteoclast in an absorption lacuna (red arrows). Osteoblasts forming bone matrix (brown arrows). Stained with methylene blue - alizarin red. x 40.

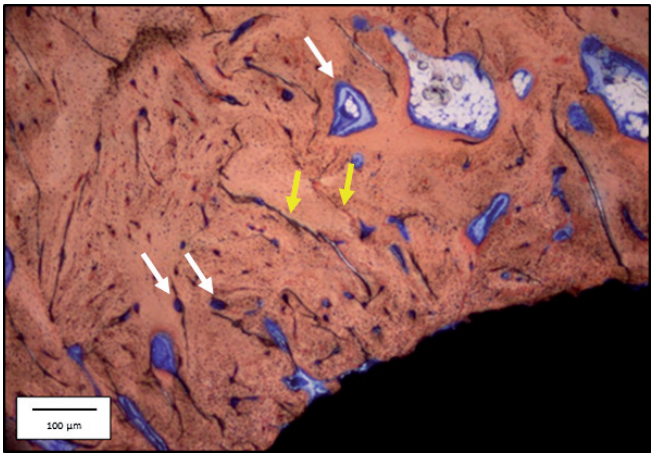

Fig. 6. Solid implant in the cortical section 12 weeks after implantation. "Mature" lamellar bone peri-implant without any histologic difference to the surrounding “genuine” mature bone. Osteoclasts cutting cones for blood vessels ingrowth (white arrows). Cement lines (yellow arrow) Stained with methylene blue - alizarin red. x 40.

peri-implant sections, which were filled in by adipose tissue (Fig. 3). A few osteoclasts were found in trough-shaped resorption lacunae (Howship's lacunae). As in the cortical section, a decreasing density of mineralized woven bone and increasing osteoid were detectable with increasing pore depth.

After 4 weeks, the newly formed bone area in a radius of +1000 µm around the implant surface decreased from the cortical to the trabecular region for both types of implant, which was only significant for PI (Table 1). In a comparison of the implant types, PI showed a significantly larger bone area in the cortical and in the trabecular area. (Table 1).

The BIC over the entire length of the implant was 28.44% (±10.89) for the SI and 26.23% (±9.07) for the PI without a significant difference (p=0.6054). The mean circumferential surface line of the raw implants was significantly lower (p<0.05) for the SI (20.08 mm ±0.25) than for the PI (28.44±3.71 mm).

12-week group

In the cortical region, the amount of osteoid was further reduced in the peri-implant region for both types of implants during the remodeling process. Less active surface osteoblasts and hardly any mesenchymal osteoblasts were detectable (Fig. 6). The osteoblasts were less flattened in appearance and aligned in a linear array on the surface of the bone structures as a sign of remodeling. Intraporous, on the other hand, the distribution pattern of the osteoid was similar to that after 4 weeks. The amount of osteoid increased significantly with increasing pore depth and accordingly a larger amount of active osteoblasts were present in the deep pores.

Both implant types were surrounded circularly and extensively by bone tissue (Figs. 6, 7). The osseoremodeling was evident by the formation of mineralized lamellar bone. The lamellar bone showed a more structured arrangement and the bony interface between the newly formed and genuine lamellar bone could no longer be distinguished microscopically (Fig. 6). An increased number of osteoclasts was found in resorption lacunae as an indication of a functional adaptation to physical strain.

The PI showed regular conversion of the initially formed woven bone into mature, mineralized lamellar bone within the pores (Fig. 7). Nevertheless, there was still a decrease of mineralized bone mass from the superficial to the deeper pores, comparable to the 4 weeks group. The matured lamellar bone has adapted more closely to the contours of the pores and to the implant surface, thereby increasing the BIC.

Table 1. Mean bone area (mm^2) of cortical and trabecular region, 4-week group.

region	solid implant	porous implant	p-value
Cortical (mm^2)	8.37±1.41	9.98±1.61	<0.05
Trabecular (mm^2)	6.98±1.18	8.45±1.74	<0.05
p-value	0.0961	<0.05	

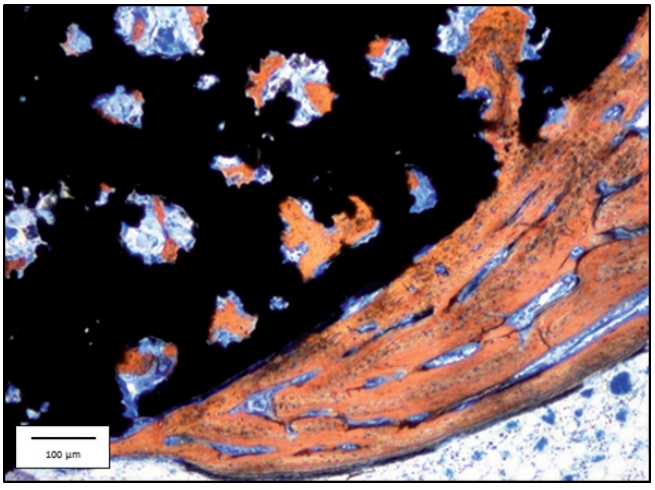

Fig. 7. Porous implant in the cortical section 12 weeks after implantation. Lamellar bone peri-implant and complete mineralization in the outer pores. Stained with methylene blue - alizarin red. x 40.

Fig. 8. Porous implant in the trabecular section 12 weeks after implantation. Columnar trabecular bone extended to the surface layers and increased their cross sections at the surface to build an anchoring foot of wider contact area. Stained with methylene blue - alizarin red. x 5.

In the trabecular region, there was less osteoblast activity around the newly formed trabecular bone and accordingly less osteoid was produced. Again, there was more osteoid in the deeper pores than near the surface.

The lamellar bone disclosed a significant lower bone area in comparison to the cortical area (Fig. 8, Table 2). However, the typical metaphyseal bone formations led to an enlargement of the bone area near the surface (Fig. 8). Columnar trabecular bone extended to the surface layers and increased their cross sections at the surface of the implant to increase the contact area. Some formations resemble an "elephant's foot" that consisted of a central osteon, from which the bone matrix extended to nestle against the implant (Fig. 9). The mineralized bone tissue showed less cellularity than after 4 weeks and the walled-in osteocytes were more organized in their formation. Bony extensions from these formations partially protrude into the pores of the PI and interlock in the pore wall like a hook or anchor (Fig. 10).

The bone area significantly decreased from the cortical to the trabecular region for SI and PI (Table 2). The cortical as well as the trabecular bone area were significantly higher for PI than for SI (Table 2).

After 12 weeks of follow-up, the mean BIC over the entire length of the implant was 47.47% (±7.47) for the SI and 42.68% (±8.83) for the PI without a significant difference (p=0.2486).

Table 2. Mean bone area (mm^2) of cortical and trabecular region, 12-week group.

region	solid implant	porous implant	p-value
Cortical (mm^2)	8.31±1.06	9.57±1.11	<0.05
Trabecular (mm^2)	5.77±1.65	7.68±1.90	<0.05
p-value	<0.05	<0.05	

Discussion

The long-term results of the successful osseointegration of an implant depend on several parameters, since an interplay of interlocking biological and mechanical factors takes place. Understanding osseointegration requires knowledge of the biology and physiology of bone, material properties and surgical techniques as well as the pathophysiology of fracture healing (Albrektsson et al., 1981; Albrektsson and Albrektsson, 1987).

In comparison to SI, PIs can improve the biological anchorage of an implant due to their surface and structure properties, which was confirmed by the results of our previous biomechanical study (Simmons et al., 1999; Otsuki et al., 2006; Li et al., 2007; Rosa et al., 2009; Vasconcellos et al., 2010; Bencharit et al., 2014; Frosch et al., 2020). Porosity affects the extent of osseointegration but there is no consensus regarding the optimum ratio of pore sizes (Jin et al., 2000; Frosch et al., 2002, 2004; Brentel et al., 2006; Vasconcellos et al., 2010). Bobyn et al. suggested an optimal pore size of 50-400 μm for bone ingrowth while others recommend a pore size of 100 to 600 μm (Bobyn et al., 1980; Karageorgiou and Kaplan, 2005; Otsuki et al., 2006; Vasconcellos et al., 2008). Karageorgiou and Kaplan suggested a minimum pore size of 300 μm, whereas Long et al. demonstrated less bone ingrowth in implants with a pore size of 960 μm compared to a pore size of 160 μm (Long and Rack, 1998; Karageorgiou and Kaplan, 2005). Long et al. postulated that the pores with 960 μm were possibly too large for favorable

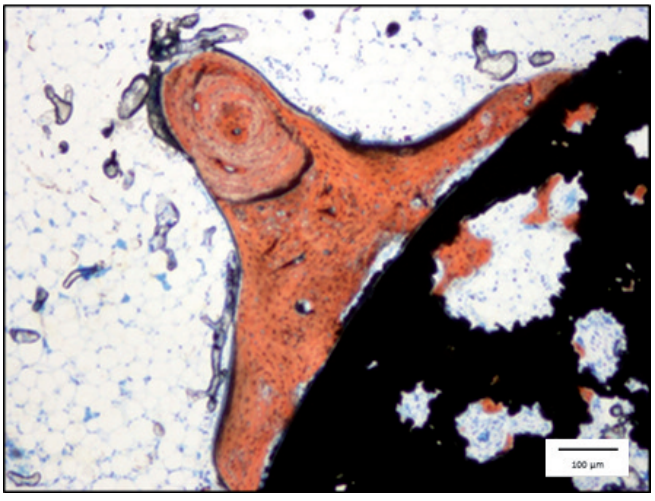

Fig. 9. Porous implant in the trabecular section 12 weeks after implantation. The mature lamellar bone formation resembles an "elephant's foot" that consisted of a central primary osteon with Haversian blood vessel (middle). Stained with methylene blue - alizarin red. x 40.

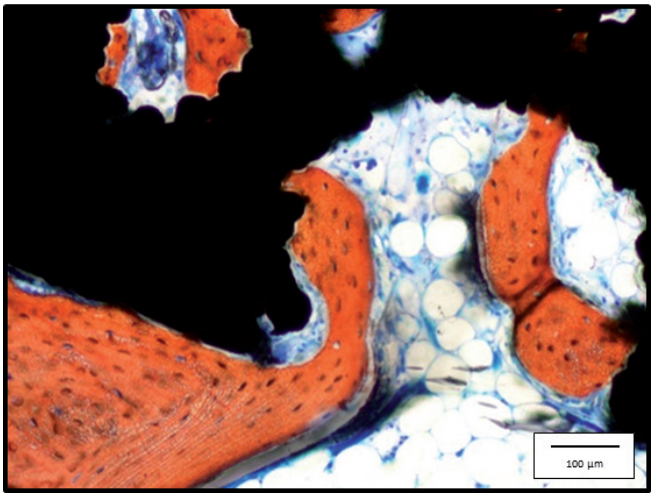

Fig. 10. Porous implant in the trabecular section 12 weeks after implantation. Mature spongiosa "anchors". Stained with methylene blue - alizarin red. x 40.

osseointegration due to insufficient surface area for cell adhesion" (Long and Rack, 1998). In the present study, the PI had a mean porosity of 49% and a pore size of 400 μm. Confluences and bridges between the paraformaldehyde spheres during the sintering process created different sized and shaped pores from 50 to 500 μm (mean 400 μm) that correspond to most of the proposed size ratios for optimal osseointegration and mimic the inhomogeneity and size relationships of trabecular bone (Hartmann, 2012; Cheng et al., 2017). Moreover, the specific mixing ration of the titanium granules shapes a rough microstructure of the pores enhancing the osteogenetic potential of the implant (Gittens et al., 2014). A pore of the PI is not a regular linear tube but by origin an irregular channel of high variability in its cross sections and contours. It may be speculated whether this variability contributes to the extent of ingrown bone towards the center of the cylinders. By scaling the manufacturing method and parameters (e.g. size and amount of the paraformaldehyde spheres or titanium granules) the presented space-holder process allows a targeted variation of the porous properties according to the desired functional and structural ability of the implant (Hartmann, 2012).

Osseointegration is a sequential process that can be roughly divided into two phases, the osseohealing and osseoremodeling (Frost, 1983; Hollister et al., 1996; Hagberg and Branemark, 2009). We have summarized the criteria for sequential osseointegration and were able to demonstrate a histomorphological regular, physiological osteogenesis both in the initial osseohealing and in the course of remodeling. After 4 weeks, the activated, mesenchymal osteoblasts were present in large numbers and predominantly embedded in synthesized osteoid. The regular sequential course was also substantiated by surface osteoblasts, which were lined up along the already developed framework of mineralized woven bone formation. Accordingly, we confirm the common definition of the initial phase of osseohealing as an excessive and spatially undirected formation of woven bone (Frost, 1983). The initial osseohealing in the rabbits is mainly completed after 4 weeks in which new bone formation and surface contact are established and an initial bony fixation of the implant is generated (Hollister et al., 1996; Marco et al., 2005; Hagberg and Branemark, 2009; Frosch et al., 2020). However, osteogenesis is to be understood as various processes on a cellular and structural level that often take place parallel to one another, whereby the respective intensity of the individual processes vary. Accordingly, we observed osteoblasts synthesizing initial formation of woven bone and at the same time osteoclasts were forming resorption lacunae as a sign of a beginning osseoremodeling after 4 weeks.

The selected metaphyseal implant site enables the examination of partial cortical and trabecular bone and provides more clinically relevant information than the diaphyseal or medullary placement alone (Sumner et al., 2001). The histological results describe a regular osteogenesis for both implant types with a physiological development of the woven bone and osteoid formations and a regular shape and arrangement of the mesenchymal as well as surface osteoblasts after 4 weeks. Overall, there were no visible differences in cell morphology between the cortical and trabecular region. However, the newly formed cortical bone area was significantly larger than the tabular bone area. A direct comparison of the values with the literature is hardly possible due to the large number of different variables (material differences, structural properties, surface modifications, animal model, implantation site, study area, staining etc). However, studies examining porous Ti-6Al-4V implants in a rabbit model showed comparable results (Cohen et al., 2017; Kuroshima et al., 2017; do Prado et al., 2018; Brogini et al., 2020; Lee et al., 2020). The lower trabecular values can be explained on the one hand by the predominantly hypodense trabecular structure and on the other hand by the lower osteogenic activity of the trabecular region in comparison to the stronger cortical region (Eschenroeder et al., 1987; Chang et al., 1994). In addition, PI showed significantly more newly formed bone area than SI regardless of region and time of examination. These results are consistent with PI's superior bone anchorage strength demonstrated in our previous biomechanical study (Frosch et al., 2020).

As part of the remodeling process, the bone areas of PI and SI decreased from 4 to 12 weeks. According to our results, He et al. and Chen et al also report of marginal bone loss in the context of remodeling (Chen et al., 2015; He et al., 2017). Histologically, the osseoremodeling was evident from a more orderly and structured mineralized lamellar bone. The increased number of osteoclasts in a variety of resorption lacunae correlate with the reduced bone area. The detection of mature, mineralized lamellar bone in the pores down to a depth of 1800 μm after 12 weeks is indirect evidence of a functional load transfer into the pores. This indicates a continuous mechanotransduction based on mechanical stimuli that influences the regulation processes of homeostasis as well osseoremodeling (Wolff, 1892; Hollister et al., 1996; Allori et al., 2008). The 3-D open porosity of the titanium framework is a basic requirement for intraporous osteogenesis as it allows vascularization and cell migration to promote bone ingrowth (Kuboki et al., 1998; Otsuki et al., 2006; Vasconcellos et al., 2008). We conclude that the open porosity further improves the osseous stabilization of PI.

In the cortical sections, the SI and PI appeared to be "walled in" by newly formed bone. In the trabecular sections, trabecular columns extended fairly perpendicular to the surface and only enlarged the cross-section near the surface by forming flat layers of bone. These flat layers had a direct contact with the implant surface. Trabeculae frequently protruded from there into the pores like a hook or anchor. The direct bone-implant contact (BIC) were similar for both types of implants

and increased significantly in the course of remodeling. These findings correspond to the increased osseous stability of the implants from 4 to 12 in our biomechanical study and to the values given in the literature, which vary roughly between 20.0% and 70% for Ti-6Al-4V implants (Cohen et al., 2016; Brizuela-Velasco et al., 2017; Cohen et al., 2017; Kuroshima et al., 2017; do Prado et al., 2018; Brogini et al., 2020; Frosch et al., 2020). The different site-specific anchoring mechanisms of cortical and trabecular bone with increasing contact area over time indicate a successful and progressive osseoremodeling process and underline the role of the BIC as a key indicator for osseointegration (Bernhardt et al., 2012; Gahlert et al., 2012). At no point in histological examinations were there any signs of inflammation, allergic reaction or infection.

Disclosure. This manuscript has not been published and is not under consideration for publication elsewhere. We have no conflicts of interest to disclose.

References

Albrektsson T. and Albrektsson B. (1987). Osseointegration of bone implants. A review of an alternative mode of fixation. Acta. Orthop. Scand. 58, 567-577.

Albrektsson T. and Zarb G.A. (1993). Current interpretations of the osseointegrated response: Clinical significance. Int. J. Prosthodont. 6, 95-105.

Albrektsson T. and Wennerberg A. (2019). On osseointegration in relation to implant surfaces. Clin. Implant. Dent. Relat. Res. 21 Suppl. 1, 4-7.

Albrektsson T., Branemark P.I., Hansson H.A. and Lindstrom J. (1981). Osseointegrated titanium implants. Requirements for ensuring a long-lasting, direct bone-to-implant anchorage in man. Acta. Orthop. Scand. 52, 155-170.

Allori A.C., Sailon A.M. and Warren S.M. (2008). Biological basis of bone formation, remodeling, and repair-part II: Extracellular matrix. Tissue. Eng. Part B Rev. 14, 275-283.

Andrew E. and Rosenberg M.D. (2004). Bones, joints, and soft tissue tumours. In: Robbins and cotran pathologic basis of disease, 7th edition. Kumar V., Abbas A.K. and Fausto N. (eds). Elsevier, Philadelphia, USA pp 1311-1314.

Bencharit S., Byrd W.C., Altarawneh S., Hosseini B., Leong A., Reside G., Morelli T. and Offenbacher S. (2014). Development and applications of porous tantalum trabecular metal-enhanced titanium dental implants. Clin. Implant. Dent. Relat. Res. 16, 817-826.

Bernhardt R., Kuhlisch E., Schulz M.C., Eckelt U. and Stadlinger B. (2012). Comparison of bone-implant contact and bone-implant volume between 2D-histological sections and 3D-srmicroct slices. Eur. Cell. Mater. 23, 237-247. discussion 247-238.

Berzins A. and Sumner D.R. (2000). Implant pushout and pullout tests. CRC Press. Boca Raton.

Bobyn J.D., Pilliar R.M., Cameron H.U. and Weatherly G.C. (1980). The optimum pore size for the fixation of porous-surfaced metal implants by the ingrowth of bone. Clin. Orthop. Relat. Res. 263-270.

Boyan B.D., Hummert T.W., Dean D.D. and Schwartz Z. (1996). Role of material surfaces in regulating bone and cartilage cell response. Biomaterials 17, 137-146.

Bram M. (2013). Pulvermetallurgische Herstellung von porösem Titan und von NiTi-Legierungen für biomedizinische Anwendungen. Schriften des Forschungszentrums Jülich

Bram M., Laptev A., Buchkremer H.P. and Stoever D. (2004). Near-net-shape manufacturing of highly porous titanium parts for biomedical applications. Mat.-wiss. u. Werkstofftechnik 35/4, Wiley-VCH, Weinheim.

Branemark P.I., Hansson B.O., Adell R., Breine U., Lindstrom J., Hallen O. and Ohman A. (1977). Osseointegrated implants in the treatment of the edentulous jaw. Experience from a 10-year period. Scand. J. Plast. Reconstr. Surg. Suppl. 16, 1-132.

Brentel A.S., de Vasconcellos L.M., Oliveira M.V., Graca M.L., de Vasconcellos L.G., Cairo C.A. and Carvalho Y.R. (2006). Histomorphometric analysis of pure titanium implants with porous surface versus rough surface. J. Appl. Oral. Sci. 14, 213-218.

Brizuela-Velasco A., Perez-Pevida E., Jimenez-Garrudo A., Gil-Mur F.J., Manero J.M., Punset-Fuste M., Chavarri-Prado D., Dieguez-Pereira M. and Monticelli F. (2017). Mechanical characterisation and biomechanical and biological behaviours of ti-zr binary-alloy dental implants. Biomed. Res. Int. 2017, 2785863.

Brogini S., Sartori M., Giavaresi G., Cremascoli P., Alemani F., Bellini D., Martini L., Maglio M., Pagani S. and Fini M. (2020). Osseointegration of additive manufacturing ti-6al-4v and co-cr-mo alloys, with and without surface functionalization with hydroxyapatite and type i collagen. J. Mech. Behav Biomed. Mater. 115, 104262.

Chang Y.S., Oka M., Kobayashi M., Gu H.O., Li Z.L., Kitsugi T. and Nakamura T. (1994). Bone formation and remodeling around implanted materials under load-bearing conditions. Clin. Mater. 17, 181-187.

Chen W.T., Han da C., Zhang P.X., Han N., Kou Y.H., Yin X.F. and Jiang B.G. (2015). A special healing pattern in stable metaphyseal fractures. Acta. Orthop. 86, 238-242.

Cheng A., Cohen D.J., Kahn A., Clohessy R.M., Sahingur K., Newton J.B., Hyzy S.L., Boyan B.D. and Schwartz Z. (2017). Laser sintered porous Ti-6Al-4V implants stimulate vertical bone growth. Ann. Biomed. Eng. 45, 2025-2035.

Cohen D.J., Cheng A., Kahn A., Aviram M., Whitehead A.J., Hyzy S.L., Clohessy R.M., Boyan B.D. and Schwartz Z. (2016). Novel osteogenic Ti-6Al-4V device for restoration of dental function in patients with large bone deficiencies: Design, development and implementation. Sci. Rep. 6, 20493.

Cohen D.J., Cheng A., Sahingur K., Clohessy R.M., Hopkins L.B., Boyan B.D. and Schwartz Z. (2017). Performance of laser sintered Ti-6Al-4V implants with bone-inspired porosity and micro/nanoscale surface roughness in the rabbit femur. Biomed. Mater. 12, 025021.

Dahl L.K. (1952). A simple and sensitive histochemical method for calcium. Proc. Soc. Exp. Biol. Med. 80, 474-479.

Diefenbeck M., Muckley T., Zankovych S., Bossert J., Jandt K.D., Schrader C., Schmidt J., Finger U. and Faucon M. (2011). Freezing of rat tibiae at -20 degrees c does not affect the mechanical properties of intramedullary bone/implant-interface: Brief report. Open Orthop. J. 5, 219-222.

do Prado R.F., Esteves G.C., Santos E.L.S., Bueno D.A.G., Cairo C.A.A., Vasconcellos L.G.O., Sagnori R.S., Tessarin F.B.P., Oliveira F.E., Oliveira L.D., Villaca-Carvalho M.F.L., Henriques V.A.R., Carvalho Y.R. and De Vasconcellos L.M.R. (2018). *In vitro* and *in vivo* biological performance of porous ti alloys prepared by powder

metallurgy. PLoS One 13, e0196169.

Eriksen E.F., Gundersen H.J., Melsen F. and Mosekilde L. (1984). Reconstruction of the formative site in iliac trabecular bone in 20 normal individuals employing a kinetic model for matrix and mineral apposition. Metab. Bone. Dis. Relat. Res. 5, 243-252.

Eschenroeder H.C. Jr, McLaughlin R.E. and Reger S.I. (1987). Enhanced stabilization of porous-coated metal implants with tricalcium phosphate granules. Clin. Orthop. Relat. Res. 234-246.

Frosch K.H., Barvencik F., Lohmann C.H., Viereck V., Siggelkow H., Breme J., Dresing K. and Sturmer K.M. (2002). Migration, matrix production and lamellar bone formation of human osteoblast-like cells in porous titanium implants. Cells Tissues Organs 170, 214-227.

Frosch K.H., Barvencik F., Viereck V., Lohmann C.H., Dresing K., Breme J., Brunner E. and Sturmer K.M. (2004). Growth behavior, matrix production, and gene expression of human osteoblasts in defined cylindrical titanium channels. J. Biomed. Mater. Res. A. 68, 325-334.

Frosch S., Nusse V., Frosch K.H., Lehmann W. and Buchhorn G. (2020). Osseointegration of 3D porous and solid ti-6al-4v implants - narrow gap push-out testing and experimental setup considerations. J. Mech. Behav. Biomed. Mater. 115, 104282.

Frost H.M. (1983). The regional acceleratory phenomenon: A review. Henry Ford Hosp. Med. J. 31, 3-9.

Gahlert M., Roehling S., Sprecher C.M., Kniha H., Milz S. and Bormann K. (2012). *In vivo* performance of zirconia and titanium implants: A histomorphometric study in mini pig maxillae. Clin. Oral. Implants Res. 23, 281-286.

Gittens R.A., Scheideler L., Rupp F., Hyzy S.L., Geis-Gerstorfer J., Schwartz Z. and Boyan B.D. (2014). A review on the wettability of dental implant surfaces ii: Biological and clinical aspects. Acta Biomater. 10, 2907-2918.

Hagberg K. and Branemark R. (2009). One hundred patients treated with osseointegrated transfemoral amputation prostheses--rehabilitation perspective. J. Rehabil. Res. Dev. 46, 331-344.

Hartmann M. (2012). Ein beitrag zur zellulären bauweise von implantatwerkstoffen nach dem vorbild der natur. Faculty of Natural Sciences and Technology III C, Pharmacy, bio and materials science, Saarland University.

He T., Cao C., Xu Z., Li G., Cao H., Liu X., Zhang C. and Dong Y. (2017). A comparison of micro-CT and histomorphometry for evaluation of osseointegration of peo-coated titanium implants in a rat model. Sci. Rep. 7, 16270.

Hollister S.J., Guldberg R.E., Kuelske C.L., Caldwell N.J., Richards M. and Goldstein S.A. (1996). Relative effects of wound healing and mechanical stimulus on early bone response to porous-coated implants. J. Orthop. Res. 14, 654-662.

Jin Q.M., Takita H., Kohgo T., Atsumi K., Itoh H. and Kuboki Y. (2000). Effects of geometry of hydroxyapatite as a cell substratum in bmp-induced ectopic bone formation. J. Biomed. Mater. Res. 52, 491-499.

Karageorgiou V. and Kaplan D. (2005). Porosity of 3D biomaterial scaffolds and osteogenesis. Biomaterials 26, 5474-5491.

Kim D.G., Huja S.S., Tee B.C., Larsen P.E., Kennedy K.S., Chien H.H., Lee J.W. and Wen H.B. (2013). Bone ingrowth and initial stability of titanium and porous tantalum dental implants: A pilot canine study. Implant Dent. 22, 399-405.

Kuboki Y., Takita H., Kobayashi D., Tsuruga E., Inoue M., Murata M., Nagai N., Dohi Y. and Ohgushi H. (1998). BMP-induced osteogenesis on the surface of hydroxyapatite with geometrically feasible and nonfeasible structures: Topology of osteogenesis. J. Biomed. Mater. Res. 39, 190-199.

Kuroshima S., Nakano T., Ishimoto T., Sasaki M., Inoue M., Yasutake M. and Sawase T. (2017). Optimally oriented grooves on dental implants improve bone quality around implants under repetitive mechanical loading. Acta Biomater. 48, 433-444.

Lee S., Chang Y.Y., Lee J., Madhurakkat Perikamana S.K., Kim E.M., Jung Y.H., Yun J.H. and Shin H. (2020). Surface engineering of titanium alloy using metal-polyphenol network coating with magnesium ions for improved osseointegration. Biomater. Sci. 8, 3404-3417.

Li J.P., Habibovic P., van den Doel M., Wilson C.E., de Wijn J.R., van Blitterswijk C.A. and de Groot K. (2007). Bone ingrowth in porous titanium implants produced by 3D fiber deposition. Biomaterials 28, 2810-2820.

Long M. and Rack H.J. (1998). Titanium alloys in total joint replacement--a materials science perspective. Biomaterials 19, 1621-1639.

Marco F., Milena F., Gianluca G. and Vittoria O. (2005). Peri-implant osteogenesis in health and osteoporosis. Micron 36, 630-644.

Marotti G., Zallone A.F. and Ledda M. (1979). Number, size, and arrangement of osteoblasts in osteons at different stages of formation. Calcif. Tissue Res. 21 [suppl], 96-101.

Otsuki B., Takemoto M., Fujibayashi S., Neo M., Kokubo T. and Nakamura T. (2006). Pore throat size and connectivity determine bone and tissue ingrowth into porous implants: Three-dimensional micro-ct based structural analyses of porous bioactive titanium implants. Biomaterials 27, 5892-5900.

Rausch G., Hartwig T., Weber M. and Schulz O. (2000). Herstellung und eigenschaften von titanschäumen [production and characteristics of titanium foam]. Mat.-wiss. u. Werkstofftechnik 31, 412-414.

Rosa A.L., Crippa G.E., de Oliveira P.T., Taba M. Jr, Lefebvre L.P. and Beloti M.M. (2009). Human alveolar bone cell proliferation, expression of osteoblastic phenotype, and matrix mineralization on porous titanium produced by powder metallurgy. Clin. Oral Implants Res. 20, 472-481.

Shapiro F. (2008). Bone development and its relation to fracture repair. The role of mesenchymal osteoblasts and surface osteoblasts. Eur. Cell. Mater. 15, 53-76.

Shapiro F. and Wu J.Y. (2019). Woven bone overview: Structural classification based on its integral role in developmental, repair and pathological bone formation throughout vertebrate groups. Eur. Cell. Mater. 38, 137-167.

Simmons C.A., Valiquette N. and Pilliar R.M. (1999). Osseointegration of sintered porous-surfaced and plasma spray-coated implants: An animal model study of early postimplantation healing response and mechanical stability. J. Biomed. Mater. Res. 47, 127-138.

Simsek I. and Ozyurek D. (2019). Investigation of the wear and corrosion behaviors of Ti5Al2.5Fe and Ti6Al4V alloys produced by mechanical alloying method in simulated body fluid environment. Mater. Sci. Eng. C Mater. Biol. Appl. 94, 357-363.

Smith L.G. and Karagianes M.T. (1974). Histological preparation of bone to study ingrowth into implanted materials. Calcif. Tissue Res. 14, 333-337.

Sumner D.R., Turner T.M. and Urban R.M. (2001). Animal models relevant to cementless joint replacement. J. Musculoskelet. Neuronal. Interact. 1, 333-345.

Sumner D.R., Turner T.M., Igloria R., Urban R.M. and Galante J.O.

(1998). Functional adaptation and ingrowth of bone vary as a function of hip implant stiffness. J. Biomech. 31, 909-917.

Vasconcellos L.M., Oliveira M.V., Graca M.L., Vasconcellos L.G., Cairo C.A. and Carvalho Y.R. (2008). Design of dental implants, influence on the osteogenesis and fixation. J. Mater. Sci. Mater. Med. 19, 2851-2857.

Vasconcellos L.M., Leite D.O., Oliveira F.N., Carvalho Y.R. and Cairo C.A. (2010). Evaluation of bone ingrowth into porous titanium implant: Histomorphometric analysis in rabbits. Braz. Oral. Res. 24, 399-405.

Vigorita J.V. (2015). Orthopaedic pathology. 3rd. Edn, Lippincott Williams and Wilkins. Philadelphia, USA.

Wolff J. (1892). Das gesetz der transformation der knochen. Hirschwald, Berlin.

Accepted March 29, 2021